2M.7 WRF SIMULATION OF THE GENESIS OF HURRICANE JAVIER (2004) IN THE EASTERN PACIFIC

Scott A. Braun
NASA/GSFC, Greenbelt, MD

1. Introduction

The Eastern Pacific has the highest frequency of genesis events per unit area of any region worldwide (Elsberry et al 1987). African easterly waves, mesoscale convective systems (MCSs), and topographic effects are thought to play roles in the genesis of tropical cyclones there (Frank and Clark 1980, Velasco and Fritsch 1987, Zehnder 1991, Zehnder and Gall 1991; Farfan and Zehnder 1997). Mozer and Zehnder (1996), using dry, idealized simulations of flow past a large-scale three-dimensional mountain range comparable to the Sierra Madre Mountains of Mexico, showed that upstream flow blocking led to diversion of the flow primarily to the south of the mountains. This flow diversion led to the formation of a low-level, barotropically unstable jet (at a location comparable to the Isthmus of Tehuantepec) and the continuous formation of synoptic-scale vorticity maxima, which they suggested may play a role in tropical cyclogenesis. Farfan and Zehnder (1997) examined the synoptic-scale circulations that led to the formation of Hurricane Guillermo (1991). Using numerical simulations, they found that flow blocking led to the formation of a low-level easterly jet south of the mountains of Central America and a northeasterly (gap flow) jet over the Gulf of Tehuantepec, which combined with the flow associated with the Intertropical Convergence Zone (ITCZ) to produce a closed cyclonic circulation in the location of Guillermo's formation. As will be discussed in this paper, the evolution of the flow field that was associated with the genesis of Hurricane Javier was similar to that described in Farfan and Zehnder (1997), with well-defined topographic flow features. Here, using a high-resolution simulation with the WRF model, we investigate whether these topographically induced flows played a significant role in the genesis of Javier.

2. Methodology

The WRF model is used with three grids (36, 12, and 4 km) in order to at least coarsely resolve the convection. The simulation is started at 12 UTC 7 September 2004, ~3 days prior to the formation of the tropical depression, and run for 3.5 days. Physics options include the Mellor-Yamada-Janjic Eta boundary layer scheme, the Monin-Obukhov (Janjic Eta) surface layer scheme, the Kain-Fritsch cumulus scheme (on the 36- and 12-km grids only) and the WSM 6-class cloud microphysics. Radiative processes are calculated every 10 minutes on the 36- and 12-km grids and every 5 min on the 4-km grid using the RRTM longwave and Goddard shortwave schemes. Initial and boundary conditions are obtained from NCEP final GFS analyses.

3. Results

This section describes the evolution of the low-level winds and precipitation and identifies several key features that, on first examination, appear to be important to the formation of the tropical depression that later became Hurricane Javier. These features include the ITCZ and its convection, two major MCSs that formed north of the ITCZ, and gap flow across the Isthmus of Tehuantepec. A primary focus here is on the role of topography in this development, in particular the gap flow in the Gulf of Tehuantepec.

Figure 1 shows the simulated radar reflectivity at 0.5 km and the surface wind vectors every 6 h for the period from 00 UTC 9 September to 00 UTC 11 September. At the first time (Fig. 1a), a broad region of convection associated with the ITCZ occurs in the southern portion of the 4-km domain. An upper-level disturbance (not shown) is beginning to move over the mountains of Honduras and Nicaragua (upper-right corner of domain) and some weak downslope flow is converging with onshore flow along the western coasts of those countries, leading to the development of convection there. This convection moves offshore (Fig. 1b) and by 12 UTC 9 September (Fig. 1c), a major MCS with a large area of northeasterly offshore flow behind (northeast of) it is present. Northerly flow through the mountain gap at the Isthmus of Tehuantepec extends almost 500 km offshore and is located to

---

Corresponding author address: Scott A. Braun, NASA/GSFC, Mail Code 613.1, Greenbelt, MD 20771.
Scott.A.Braun@nasa.gov

the west of the MCS. By 18 UTC (Fig. 1d), the MCS begins to weaken and by 00 UTC 10 September (Fig. 1e), its remnants are moving to the west ahead of a region of strong southeasterly flow in the coastal zone at low levels and ahead of a mesoscale vortex at midlevels (not shown). The remnants of the MCS redevelop into an intense squall line oriented perpendicular to the coast and moving ahead of the strong southeasterly winds (Fig. 1f). It moves into the region of the northerly gap flow by 12 UTC 10 September (Fig. 1g). The combination of northwesterly flow in the northwestern-most part of the domain, northerly gap flow, an increasing area of southeasterly flow in the coastal zone behind and to the south of the squall line, and south-southwesterly flow south of the ITCZ, all come together to produce a broad area of cyclonic flow at the surface, in a manner similar to that described by Farfan and Zehnder (1997) for Hurricane Guillermo. At later times (Figs. 1h and 1i), both the surface cyclonic circulation and the surrounding convection become better organized to form the tropical depression.

Many of these features are observable in GOES and Quikscat satellite imagery. GOES data (not shown) confirm the early development of convection in the coastal zone, although with a more complete dissipation of the MCS by 00 UTC 10 September (cf. Fig. 1e). GOES data show the subsequent development of the squall line oriented perpendicular to the coast around 06 UTC and its movement west-northwestward. The GOES data also show a major MCS to the south of the squall line, possibly along the ITCZ, which is not well reproduced by the model. The squall line and the MCS later merge, in a manner similar to that shown in Figs. 1g-1i, to form the tropical depression. Quikscat data on 9-10 September (not shown) reveal the presence of a persistent gap flow, the offshore flow contributing to the early MCS, the surge of southeasterly flow behind the squall line, and the eventual organization of the depression circulation.

The evolution of the surface winds fields, particularly in regards to the gap flow in the Gulf of Tehuantepec and the strong southeasterly winds in the coastal zone, are highly suggestive of a role of the topography in the formation of the tropical depression. In order to ascertain what role topography may play, two additional experiments are conducted in which portions of the topography of Central America are removed. In the first experiment, called NOTOPO1, the mountains extending from the Isthmus of Tehuantepec to Panama are removed (Fig. 2b). The second experiment (NOTOPO2) is similar to NOTOPO1, but also eliminates the southern portion of the Sierra Madre mountains (Fig. 2c) in order to examine the role of the gap flow. Results of these experiments are shown in Figs. 2d-2i, where simulated radar reflectivities and sea-level pressure at the end of the simulation (00 UTC 11 September) are compared to the control run.

The evolution of the winds and precipitation in the NOTOPO1 experiment are very similar to the control run except that the strong southeasterly flow does not develop in the coastal zone behind the MCS; instead, stronger northeasterly flow occurs ahead of the MCS (not shown). By the end of the simulation (Fig. 2, middle panels), the tropical depression has formed, has a somewhat better organized cyclonic circulation, and is slightly stronger (in terms of the minimum sea-level pressure) than in the control run (Fig. 2, left panels). Thus, while the mountains account for the southeasterly winds in the coastal zone, this flow is apparently not critical for cyclogenesis. The biggest difference between the simulations at this time is seen in the direction of the gap flow in the Gulf of Tehuantepec.

The purpose of the NOTOPO2 run is to test the importance of the gap flow on the storm development. By removing the southern end of the Sierra Madre mountains, the flow around their southern end is shifted significantly northward away from the developing storm. The evolution of the precipitation is again similar to the control run, but with some key differences toward the end of the simulation. Because there is no longer a gap flow in the low-level winds, the squall line advancing northwestward along the coast moves into a more quiescent environment. Whereas in the control and NOTOPO1 runs the interaction between the squall line and the northerly gap flow ahead of it helps to maintain the linear organization, in the NOTOPO2 run the line quickly breaks down into a more circular, less organized structure. This change leads to a tighter, more intense cyclonic circulation and lower sea-level pressure (Fig. 2, right panels) by the end of the simulation.

4. Summary

The WRF model was able to fairly accurately reproduce many features of the genesis process observed by satellite. Genesis did not result from the mesoscale vortex of a single MCS, but instead appeared to result from the merger of flows associated with several MCSs. Although not discussed here, processes associated with the ITCZ also were important. The simulated low-level flow patterns were highly suggestive of a role of topographically induced flows such as the gap flow through the Isthmus of Tehuantepec. However, experiments that removed portions of the topography clearly indicated that, at least for Hurricane Javier, the topographic effects did not aid formation and, in fact, actually inhibited development to a limited extent. The analysis is currently very preliminary and further work is needed to determine the roles of synoptic-scale processes as well as mesoscale and convective scale vortex-merger processes.

Elsberry, R. L., W. M. Frank, G. J. Holland, J. D. Jarrell, and R. L. Southern, 1987: *A Global View of Tropical Cyclones.* University of Chicago Press, 185 pp.

Farfan, L. M., and J. A. Zehnder, 1997: Orographic influence on the synoptic-scale circulations associated with the genesis of Hurricane Guillermo (1991). *Mon. Wea. Rev.*, **125**, 2683-2698.

Frank, N. L., and G. Clark, 1991: Atlantic tropical systems of 1979. *Mon. Wea. Rev.*, **108**, 966-972.

Mozer, J. B., and J. A. Zehnder, 1996: Lee vorticity production by large-scale tropical mountain ranges. Part I: Eastern North Pacific tropical cyclogenesis. *J. Atmos. Sci.*, **53**, 521-538.

Velasco, I., and J. M. Fritsch, 1987: Mesoscale convective complexes in the Americas. *J. Geophys. Res.*, **92**(D), 9591-9613.

Zehnder, J. A., 1991: The interaction of planetary-scale tropical easterly waves with topography: A mechanism for the initiation of tropical cyclones. *J. Atmos. Sci.*, **48**, 1217-1230.

Zehnder, J. A., and R. A. Gall, 1991: Alternative mechanisms of tropical cyclone formation in the eastern North Pacific. *Atmósfera*, **4**, 37-51.

FIGURE CAPTIONS

Figure 1. Simulated radar reflectivity from the 4-km grid at 0.5 km mean sea level and surface winds for the control simulation at 6-h intervals from 00 UTC 9 September (hour 36 of the simulation) and 00 UTC 11 September. Latitude/longitude lines are drawn every 5°. The solid lines represent the coastlines of Central America from southern Mexico to northern Costa Rica.

Figure 2. Simulation results for (left panels) the control run, (middle panels) NOTOPO1, and (right panels) NOTOPO2. (Top panels) Terrain height from the 36-km grid showing the modifications to topography in the NOTOPO1 and NOTOPO2 runs. The red boxes indicate the locations of the 4-km grids shown in other panels. Latitude/longitude lines are drawn every 10°. (Middle panels) Same as in Figure 1, but showing results for 00 UTC 11 September for the three simulations. (Lower panels) Similar to the middle panels, but showing sea-level pressure (at 1 mb intervals) and surface winds.

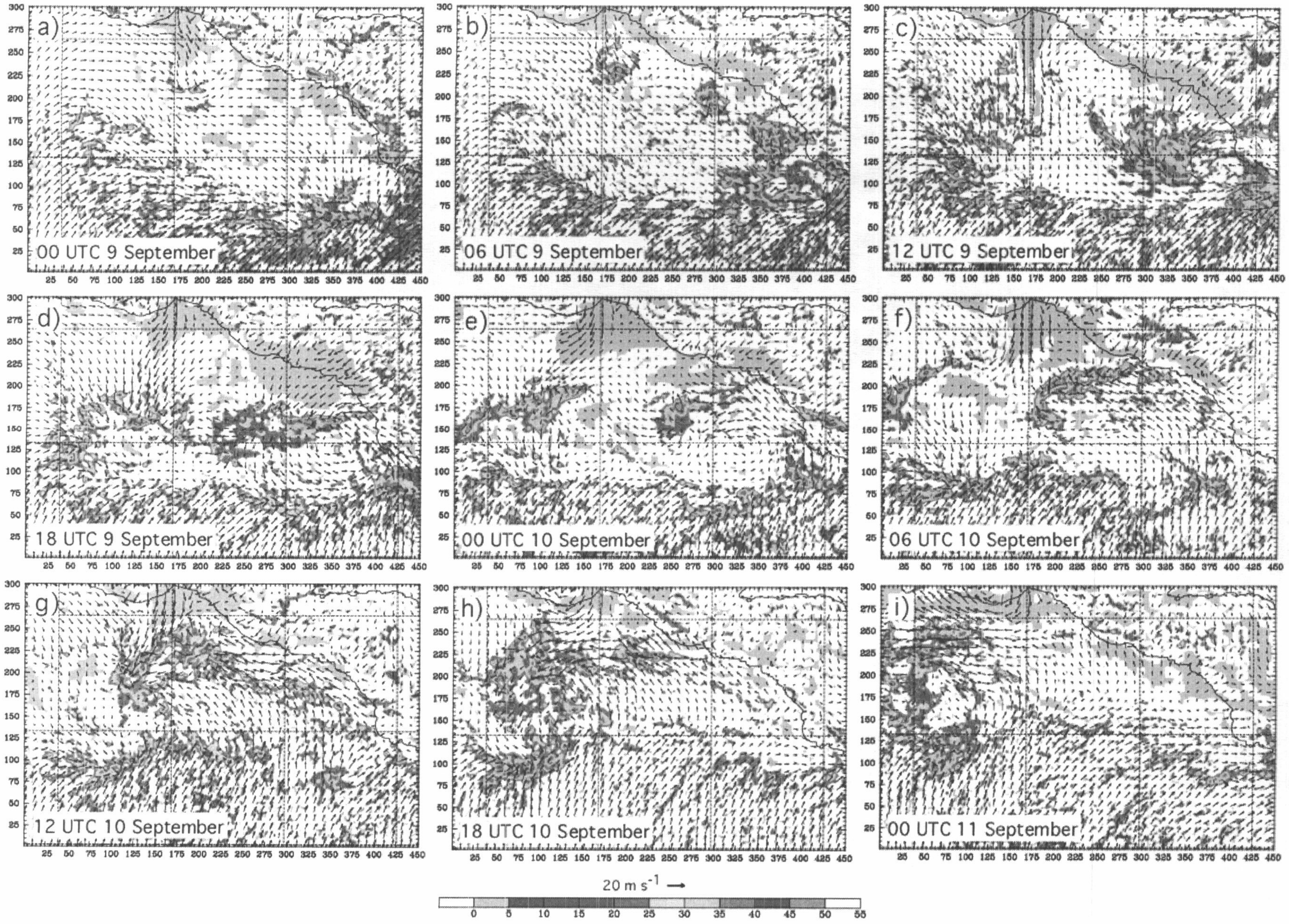
a)
00 UTC 9 September
b)
06 UTC 9 September
c)
12 UTC 9 September
d)
18 UTC 9 September
e)
00 UTC 10 September
f)
06 UTC 10 September
g)
12 UTC 10 September
h)
18 UTC 10 September
i)
00 UTC 11 September
25 50 75 100 125 150 175 200 225 250 275 300 325 350 375 400 425 450
300 275 250 225 200 175 150 125 100 75 50 25
20 m s^{-1} →
0 5 10 15 20 25 30 35 40 45 50 55

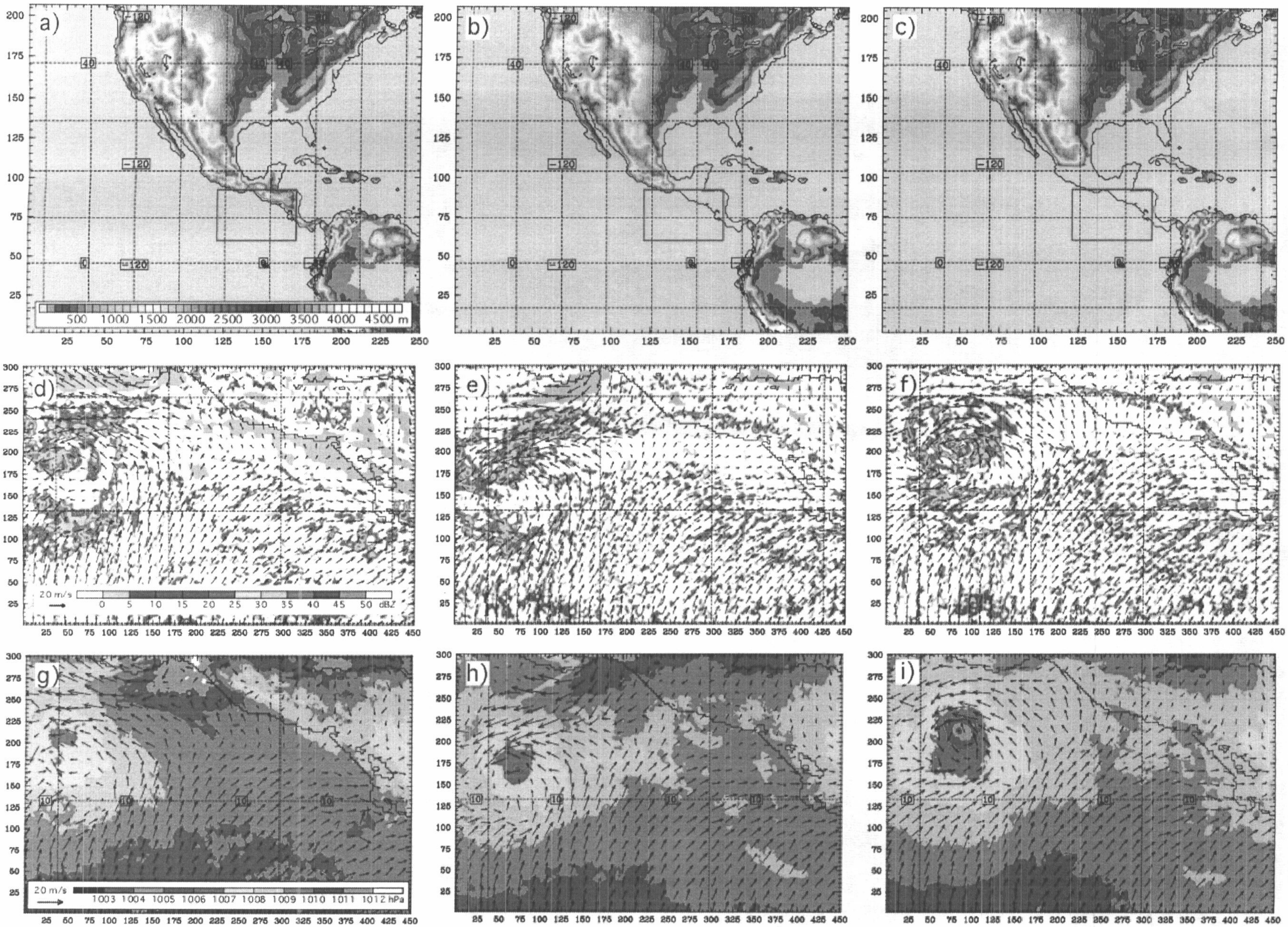a)
b)
c)
d)
e)
f)
g)
h)
i)
40
−120
0
500 1000 1500 2000 2500 3000 3500 4000 4500 m
20 m/s
0 5 10 15 20 25 30 35 40 45 50 dBZ
10
1003 1004 1005 1006 1007 1008 1009 1010 1011 1012 hPa
25 50 75 100 125 150 175 200 225 250
25 50 75 100 125 150 175 200 225 250 275 300 325 350 375 400 425 450